De Gruyter Brill
Paradigm
ISSN 1335-8871

MEASUREMENT SCIENCE REVIEW

Journal homepage: https://reference-global.com/journal/MSR

Test and Analysis of the Influence of Lake Water Obstacle on the Near-field Timing Signal of BPC

Fan Zhao[1,2,3,4], Luxi Huang[1,3,4], Xin Wang[1,3,4], Zhen Qi[1,2,3,4], Xiaoqian Ren[1,3,4], Ping Feng[1,2,3,4*], Yu Hua[1,2,4]

[1]*National Time Service Center (NTSC), Chinese Academy of Sciences, Xi'an, 710600, China, zhaofan@ntsc.ac.cn, huangluxi@ntsc.ac.cn, wangx@ntsc.ac.cn, qizhen@ntsc.ac.cn, renxq@ntsc.ac.cn, pingfp@ntsc.ac.cn, hy@ntsc.ac.cn*
[2]*University of Chinese Academy of Sciences, Beijing, 100049, China*
[3]*Fengkai Low-Frequency Time Code Time Service Station, Zhaoqing, 526500, China*
[4]*Key Laboratory of Time Reference and Applications Chinese Academy of Sciences, Xi'an, 710600, China*

Abstract: The lake water environment is a common and complex scenario for the application of radio time synchronization. When the timing signal enters lake water, signal strength attenuation and phase shift occur, which greatly affect time service performance. By comparing the differences in signal field strength and time difference at the same distance from the transmitting station along two different direction paths – one through soil and the other through lake water – the influence of the freshwater lake transmission medium on the propagation of BPC timing signals within the ground wave range was analyzed. This paper uses the BPC timing signal as an example to describe the propagation mode and attenuation characteristics of the signal when it enters the lake water environment, and establishes a BPC field strength and time difference measurement system to analyze possible field strength and time difference variation laws of the BPC timing signal at different propagation distances in lake water. Studies show that at a distance of 25 km from the transmitting station, when the signal passes through lake water, the field strength attenuation is approximately 0.24 dBμV/m and the time difference increases by approximately 8.04 μs. At a distance of 138 km from the transmitting station, when the signal passes through lake water, the field strength attenuation is approximately 0.6 dBμV/m and the time difference increases by approximately 14.1 μs.

Keywords: BPC, low-frequency time-code, ground wave, field strength

1. INTRODUCTION

At present, the time service system can be divided into two parts: satellite-based time service systems and ground-based time service systems. The former mainly refers to the Global Navigation Satellite System (GNSS) satellite time service system, which offers high precision, wide coverage, low cost and convenient operation, and has been widely used in various fields [1]. The latter mainly includes the long-wave time system (BPL), short-wave time system (BPM), and BPC system (BPC), with timing accuracy ranging from micro-seconds (μs) to milliseconds (ms), and is mainly used by military and civilian users [2].

Although satellite navigation systems provide high-precision timing services and are widely used, their vulnerability to occlusion and interference remains a drawback. These potential safety hazards and shortcomings have limited their development. The BPC, which has the lowest timing cost among the ground-based time service systems, offers strong anti-interference capability and high stability, serving as a backup and supplement to the satellite-based time service system [3]. Low-frequency time-code timing technology has many advantages, but in complex environments such as valleys, forests, rivers, lakes, and other terrain areas, the propagation characteristics of low-frequency time-code timing signals are not yet known. Therefore, this paper selects lakes as a typical scenario to study the propagation characteristics of low-frequency time-code timing signals. According to the characteristics of BPC, the signal strength gradually decreases as the transmission distance increases and reaches its optimal value within the ground wave range. However, there are also some external interferences affecting the timing service of BPC in near-field waves, making it necessary to conduct further tests and research.

Researchers have studied and explored the influence mechanisms of underwater radio transmission systems in marine environments, analyzing the effects of water conductivity, salinity, and temperature on the efficiency of

DOI: 10.2478/msr-2026-0004

*Corresponding author: pingfp@ntsc.ac.cn (P. Feng)

radio energy transmission. They found that highly conductive seawater increases signal attenuation [4]. The conductivity and absorption characteristics of water have a significant impact on the propagation of radio signals, especially in the low-frequency band [5]. Research on the propagation characteristics of low-frequency signals in shallow sea environments found that changes in water conductivity significantly affect the propagation path and attenuation of signals [6]. The latest progress in underwater wireless optical communication technology is reviewed, discussing the influence of the optical and propagation characteristics of water on wireless optical communication. The article mentions that the absorption and scattering characteristics of water significantly affect the propagation distance and quality of the signal [7]. Due to the absorption and scattering effects of the water body itself and the impurities it contains on the signal wave, various parameters of the signal wave, such as intensity, spatial characteristics, polarization characteristics, etc., are changed [8]. Reflection and refraction at the water surface and bottom can change the propagation direction of electromagnetic waves, increasing signal attenuation and distortion [9]. Changes in soil conductivity can also alter the propagation path of radio signals [10].

Within the range of ground wave radio propagation, changes in the conductivity of vegetation alter the propagation environment for very low-frequency signal (VLF) signals. In areas covered with vegetation, the conductivity of the vegetation can affect both the propagation path and the attenuation of the signal. Singh et al. found that changes in vegetation conductivity can also affect the stability of VLF signals. In regions where vegetation conductivity varies significantly, signal propagation may experience increased interference and fluctuations, leading to decreased signal stability [11]. Korsakov [12] reported that in Yakutsk, when recording signals from the Novosibirsk transmitters, increased permeability of the upper soil layer – caused by the melting of snow cover in summer and the thawing of the upper layer of frozen soil, which changed the soil's electrical conductivity – led to a decrease in atmospheric electric field intensity during summer. In winter, the soil froze and the moisture decreased, resulting in increased soil resistivity. This reduced ground conductivity, causing less attenuation of the VLF signal during propagation. Zhao et al. described the propagation laws of low-frequency signals in both sky wave and ground wave regions, as well as the effects of natural events such as earthquakes on signal field strength and phase [13].

Based on the above background, this paper presents a systematic analysis of the composition, structure, transmission, and characteristics of BPC. A test method is proposed, and an experimental system is built to test the timing services of different transmission media in the BPC ground wave area. In an actual lake water environment, two lake locations, 25 km and 138 km from the transmitting station, were selected. Tests were conducted in groups, and the relative changes in the field strength of the BPC timing signal in different directions and along different transmission paths were compared. Finally, a conclusion was drawn.

2. SUBJECT & METHODS

A. BPC time service system

The National Time Service Center (NTSC), Chinese Academy of Sciences, built a BPC time service station in Shangqiu City, Henan Province, in 2008. The call sign is BPC, and the transmission power is 100 kW. The broadcasting frequency of BPC radio is 68.5 kHz. At the start of each full second, the pulse amplitude drops to 90 % of the original amplitude. The widths of the falling pulses are 100 ms, 200 ms, 300 ms and 400 ms, respectively. As shown in Fig. 1, BPC uses a pulse width modulation signal format as its signal structure, and the passband is 67.5 kHz to 69.5 kHz.

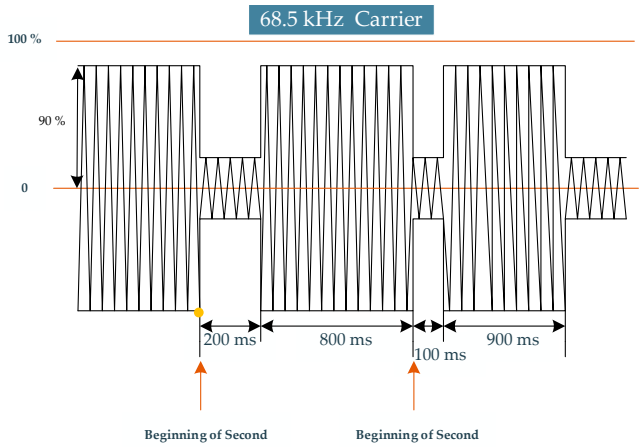

Fig. 1. The waveform of the BPC signal.

B. Ground wave propagation mechanism

The propagation mechanism of low-frequency radio timing ground waves involves the characteristics of electromagnetic waves traveling along the Earth's surface and their unique advantages in the low-frequency band. Ground waves are electromagnetic waves that propagate along the Earth's surface. Their propagation distance is affected by frequency, surface electrical properties (conductivity, dielectric constant), and terrain. Generally, ground waves are not affected by climate, have high reliability, but their propagation distance is limited. When radio waves travel along the ground, the induced charges on the ground move with the changes of the waves, forming a current. Due to certain resistance of the ground, energy is consumed as the current passes through. This effect is especially pronounced for horizontally polarized waves, whose electric field is parallel to the ground; the resulting current in the ground is large, leading to significant energy loss. To better couple with the ground and achieve long-distance propagation, vertically polarized waves are used for ground wave propagation, and vertical antennas are employed for transmission and reception [14], [15]. Fig. 2 shows a model illustrating the principle of ground wave propagation.

The field strength of ground wave signal propagation (dB) can be expressed as

$$E = 109.54 + A - 20 \cdot \lg d + 10 \cdot \lg P_{\Sigma} \qquad (1)$$

In this formula, d is the spatial path of wave propagation (large circle distance), A is the attenuation coefficient on the ground, and $P_{\sum}$ is the radiation power of the transmitting antenna, measured in kW. The constant 109.54, expressed in logarithmic units, represents the electromagnetic field intensity (300 mV/m) at a distance of 1 km from the transmitting station with a transmission power of a short unipolar antenna of 1 kW.

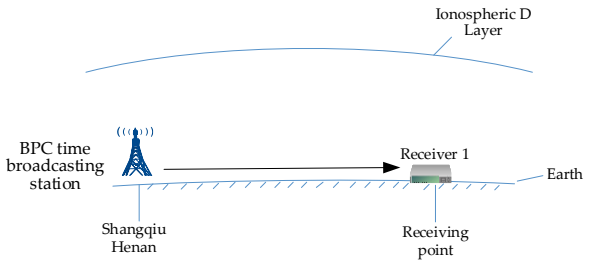

Fig. 2. Principle model of ground wave propagation.

C. Performance parameters

According to the principles of radio waves and antennas, when the polarization direction of the antenna in the air matches that of the measured signal, the antenna will receive the maximum induced signal. The measurement of field strength can thus be converted into the measurement of the magnitude of the induced signal, specifically the amplitude of the electrical signal, enabling the measurement of the electrical signal. The field strength tester is designed with a magnetic antenna to measure field strength [16]. According to the fundamental laws of electromagnetism, the induced voltage of a coil placed in a spatial magnetic field is:

$$e_S = \omega \cdot B \cdot A \cdot N \tag{2}$$

Here, ω is the angular frequency of the induced voltage, B is the density of the magnetic field lines in free space, A is the area of the coil, and N is the number of turns of the coil.

If magnetic rod A with an effective magnetic permeability coefficient of μ_i is inserted into the coil, the induced voltage becomes e_S

$$e_S = \omega \cdot B \cdot A \cdot N \cdot \mu_i \tag{3}$$

For an electromagnetic wave traveling in the A plane, in free space, the field strength of the electromagnetic field can be characterized by the electric field intensity E (V/m) or the magnetic field intensity H (A/m) [17].

$$E/H = 120 \cdot \pi \approx 377\ \Omega \tag{4}$$

$$B = \mu \cdot H \tag{5}$$

Here, E is the electric field intensity, H is the magnetic field intensity, μ is the magnetic permeability in free space $(4\pi \cdot 10^{-7}\mathrm{H/m})$ and ε is the dielectric constant in free space $(\frac{1}{36 \cdot \pi} \cdot 10^{-9}\ \mathrm{F/m})$

Substituting (4) and (5) into (3), we obtain

$$e_S = \omega \cdot \frac{E}{120 \cdot \pi} \cdot \mu \cdot A \cdot N \cdot \mu_i \tag{6}$$

Here,

$$\omega = \frac{2 \cdot \pi \cdot C}{\lambda}$$

$C = 299792.5\ \mathrm{km/s}$, C for the speed of light.

That is:

$$e_S = \frac{2 \cdot \pi}{\lambda} \cdot \frac{C \cdot \mu}{120 \cdot \pi} \cdot A \cdot N \cdot \mu_i \cdot E \tag{7}$$

In the formula,

$$\frac{C \cdot \mu}{120 \cdot \pi} \approx 1$$

$$e_S = \frac{2 \cdot \pi \cdot A \cdot N \cdot \mu_i}{\lambda} \cdot E \tag{8}$$

In the formula, A, N, μ_i are determined by calculation based on the received carrier frequency of 68.5 kHz, providing a theoretical basis for obtaining the electric field intensity E.

Signal field strength is a physical quantity that represents the intensity and direction of an electric field and is an important indicator of the electromagnetic environment. In the performance characterization of BPC, the signal field strength reflects the signal quality of the receiver environment and also affects the 1PPS synchronization accuracy to some extent. Therefore, it is the core indicator for testing the timing performance of BPC.

We have established a test experimental system for measuring the time difference of BPC timing. The test method is shown in Fig. 4.

The rubidium clock provides a 10 MHz reference signal to the BPC receiver, GNSS receiver, and time interval counter, ensuring all devices are locked to the same frequency reference. The 1PPS output from the GNSS receiver is synchronized with GNSS time. The difference between GNSS time and UTC (NTSC) is always within 20 ns and can be ignored in experiments. The 1PPS output of the GNSS receiver is used as the reference, and the 1PPS output of the BPC receiver is used as the measurement time. The time interval counter measures the time deviation between the 1PPS outputs of the GNSS receiver and the BPC receiver, representing the time difference, that is, the link delay time from the BPC broadcasting station transmitter to the receiver. The experimental system operates stably. We used a computer to collect the time difference data output of the time interval counter.

Based on this, we built an experimental system to test the timing service within the near-field and ground wave range of BPC, as shown in Fig. 3 and Fig. 4.

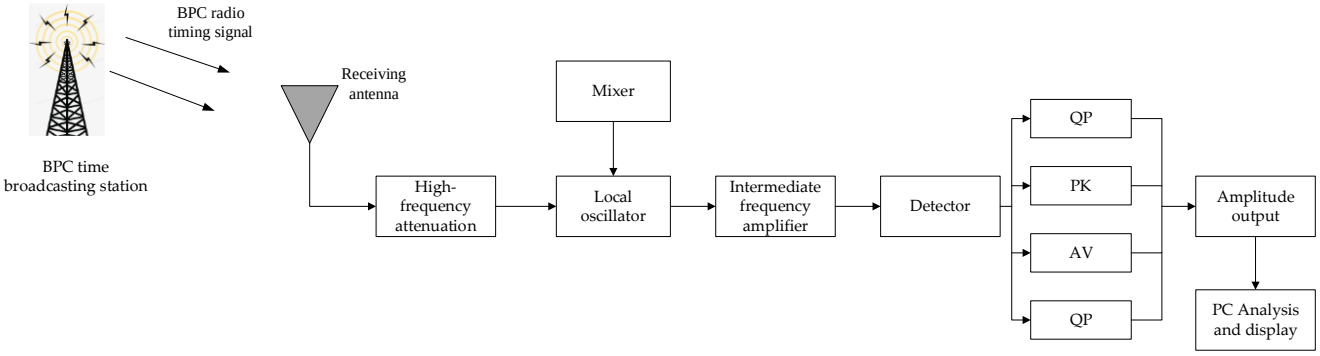

Fig. 3. Test method for field strength of BPC near-field timing signal.

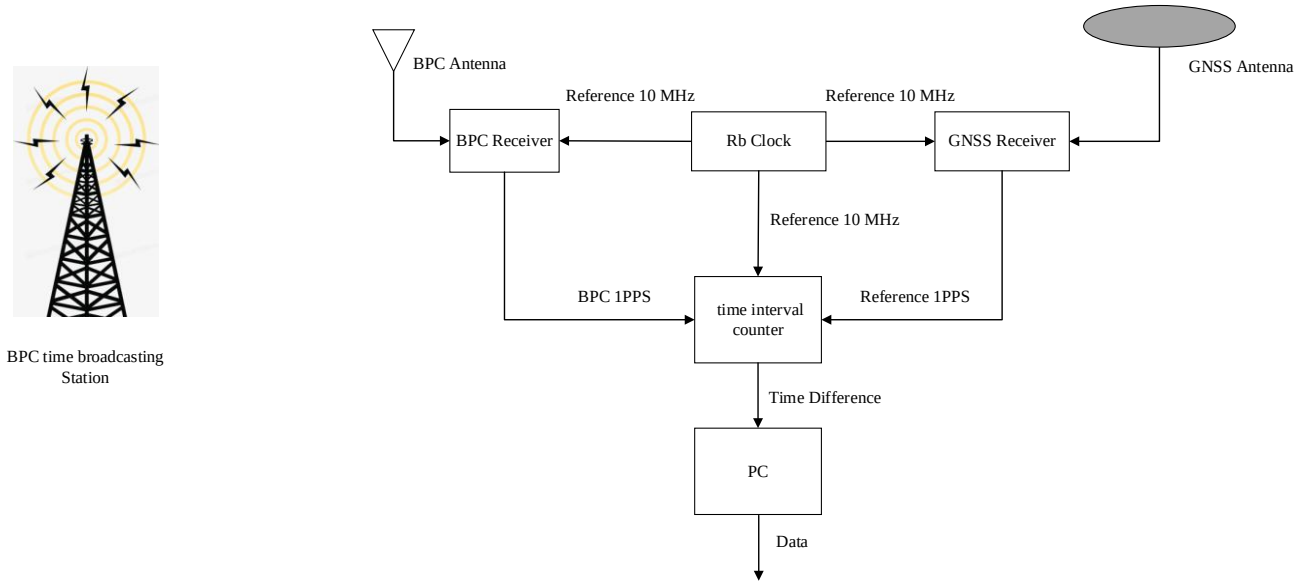

Fig. 4. Test method for time difference of BPC timing signal.

D. Experimental method and data source

Let us convert the field strength measurement of the BPC timing signal into a measurement of the amplitude of the induced signal. After amplifying and filtering the signal from the antenna, the amplitude of the digitized signal is tested and calculated. By selecting an appropriate threshold and eliminating outliers and interference data, the field strength of the BPC timing signal can be obtained [18].

The experimental group established a BPC timing signal measurement system, which consists of an antenna receiving module and a signal processing and display module, as shown in Fig. 3. The circular magnetic antenna of the electromagnetic interference interferometer receives BPC timing signals with a carrier frequency of 68.5 kHz [19]. The antenna receives the BPC timing signal, which then passes through the radio frequency circuit. After mixing, amplification, detection, and filtering, the field strength is obtained. The signal processing and display module processes the data, and the real-time measurement data is collected and stored through the upper computer software [20].

To assess how lakes affect the BPC timing signal in the ground wave region, the experiment was conducted in two directions. Two lakes were selected : Fulong Lake, located approximately 25 km from the station within Shan County, Heze City, Shandong Province, China. Fulong Lake lies within the ancient course of the Yellow River, covers a water area of 21 square kilometers, and has an average depth of 3.5 meters. The second lake is Weishan Lake, located 138 km from the station in southern Shandong Province, China. Weishan Lake is a large freshwater lake and one of the largest freshwater lakes in northern China, stretching 120 km in length and 6 to 25 km in width. Its surface area is approximately 660 km² at normal water levels, expanding to about 1266 km² during peak flood periods. The average depth is 1.5 m, with a maximum depth of 6 m, making it a dynamic freshwater lake system. Weishan Lake serves as a critical passage for the Eastern Route of China's South-to-North Water Diversion Project and functions as a riverine lake, undergoing a complete dynamic cycle of inflow, storage, outflow, and water diversion. The testing methods around both lakes were identical. To minimize and eliminate the influence of the ionosphere as much as possible, the test was conducted at noon, the most stable time for the ionosphere in the test country. The test lasted approximately one hour. The method for measuring the field strength of the BPC ground wave range timing signal is shown in Fig. 5.

The BPC measurement system was placed sequentially at Test point 1 (where the signal passes through the lake) and Test point 2 (where the signal does not pass through the lake) to measure the field strength of the BPC timing signal. The distances $d1$ and $d2$ from the BPC transmitter to test points 1 and 2, respectively, were equal. The field strength variation characteristics of the low-frequency time-code timing signal in the near-field range of the ground wave at equal distances and in different directions along different paths were explored.

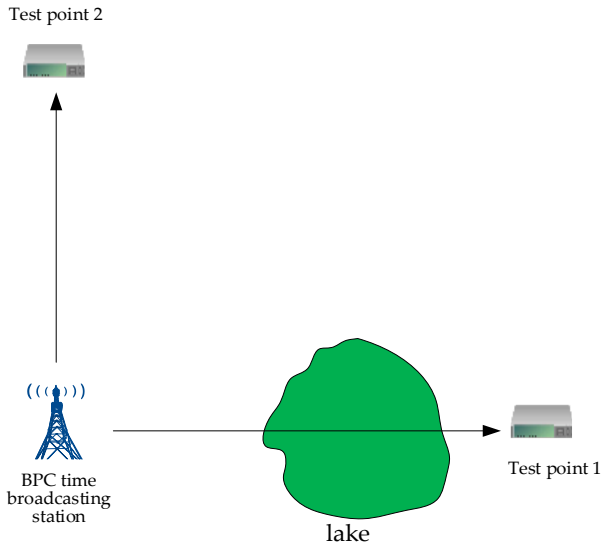

Fig. 5. Test principle diagram for test point selection.

3. RESULTS

By integrating all these devices into a portable mobile test system, we can easily test the BPC timing service at any location under different environmental conditions. Since the experimental system operates stably, we use a computer to collect waveform field strength and time difference data. Based on comprehensive data analysis and evaluation, the following test results are reported.

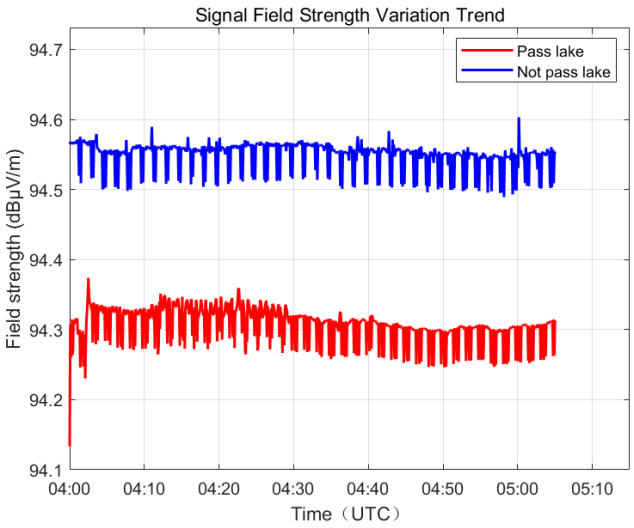

Fig. 6. Comparison chart of the first group of lake water field strength values.

The test situation for the first lake water in the ground wave area is shown in Table 1. The two test points are very close to the transmitter, but the propagation path environments where the test equipment is located differ. The test duration at each test point is about 1 hour.

Table 1 shows that the field strength is greatest along the path not passing through the lake water, which is 0.24 dBμV/m stronger than the average field in the direction passing through the lake water. The detailed test data for the ground wave area are shown in Fig. 6, where the red curve represents the field strength results in the direction passing through the lake water, and the blue curve represents the test results without passing through the lake water. It can be seen from Fig. 6 that both groups of measured data are relatively stable. The differences between the maximum and minimum values are 0.24 dBμV/m and 0.11 dBμV/m, respectively, and the standard deviations are 0.0249 and 0.0183, respectively. This indicates that after passing through the lake water, there is a slight fluctuation in the signal field strength, and the field strength range also increases accordingly. The skewness of both groups of data is negative, indicating that the data distribution has a longer left tail, meaning there are more extremely small values on the left side. This means that most of the data are concentrated on the side with larger values, while the data with smaller values are fewer but more scattered. The kurtosis of the two groups of data is relatively close, indicating that the measurement of the peak and the flatness of the data distribution curves are basically the same.

Table 1. Statistics of test data for the lake test within the near-field range (25 km).

Statistics of filed strength [dBμV/m]	Test point 1 Pass lake	Test point 2 Not pass lake
Max value	94.37	94.60
Min value	94.13	94.49
Peak_to_peak	0.24	0.11
Mean value	94.31	94.55
Std	0.0249	0.0183
Skewness	–1.07	–1.67
Kurtosis	5.75	5.12
Energy	6954916.50	6990942.66

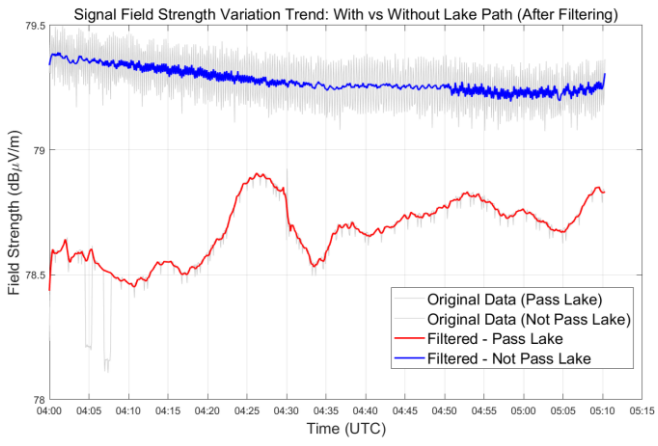

Fig. 7. Comparison chart of lake water field strength values in the second group (After filtering).

We conducted signal field strength tests at two locations 138 km from the broadcasting station. The raw data underwent 3 σ outlier processing and smoothing filtering, effectively eliminating "spikes" and "jumps." The filtered field strength trend diagram is shown in Fig. 7.

Statistical analysis of the filtered data is presented in Table 2.

Table 2. Statistics of test data for the lake test within the ground wave range (138 km).

Statistics of filed strength [dBμV/m]	Test point 1 Pass lake	Test point 2 Not pass lake
Max value	78.91	79.39
Min value	78.43	79.19
Peak_to_peak	0.48	0.20
Mean value	78.68	79.28
Std	0.1170	0.0456
Skewness	–0.0907	0.6331
Kurtosis	3.0129	2.3757
Energy	5224486.12	5304515.55

The test results for the second group of lake water in the ground wave area are shown in Table 2. Compared with the first lake water scenario, the distance between the two test points and the BPC transmitter station is greater, resulting in relatively weaker signal strength. Both locations are within the pure ground wave range. According to the transmission law of low-frequency signals, this range is dominated by ground wave propagation, and the signal field strength does not depend on the ionosphere. It is mainly influenced by factors such as the earth's electrical conductivity of the ground wave medium, the moisture, salt, and mineral content in the soil, terrain, and obstacles. Similarly, two test points on different propagation paths were selected, and the test duration for each test point was approximately one hour.

As shown in Table 2, the field strength is highest along the path that does not pass through the lake, exceeding the average field strength in the lake-passing path direction by 0.6 dBμV/m. The raw test data for the second group in the ground wave region are represented by the gray line, while the data after median smoothing filter processing for the second group are shown in Fig. 7. Fig. 7 presents the filtered field strength values: the red curve represents the filtered results for the lake-water path direction, while the blue curve shows the filtered results for the non-lake-water path direction. As seen in Fig. 7, the blue curve's measured data exhibit greater stability compared to the red curve. The difference between the maximum and minimum values in the two groups is 0.48 dBμV/m and 0.2 dBμV/m, respectively, with standard deviation values of 0.1170 and 0.0944. This indicates that the signal field strength exhibits significant fluctuations after passing through the lake, and the range of field strength also increases accordingly. As the distance from the test point to the broadcasting station increases, this fluctuation range becomes more pronounced. Test Point 1 exhibits negative skewness, while Test Point 2 shows positive skewness, revealing asymmetric distributions between the two datasets. This contrasts markedly with the dataset closer to the transmission station, indicating that within the ground wave range, varying distances from the station and differing propagation paths significantly alter the BPC signal field strength. After applying smoothing filters to the data, the kurtosis values for the two sets were greater than 3 and less than 3, respectively. This indicates the degree of peak measurement in the data distribution and the differing flatness of the distribution curves. It is evident that the field strength propagating through the lake water path exhibits an uneven curve.

The time difference comparison test was conducted on the first group, Fulong Lake, and the test results are shown in Fig. 8.

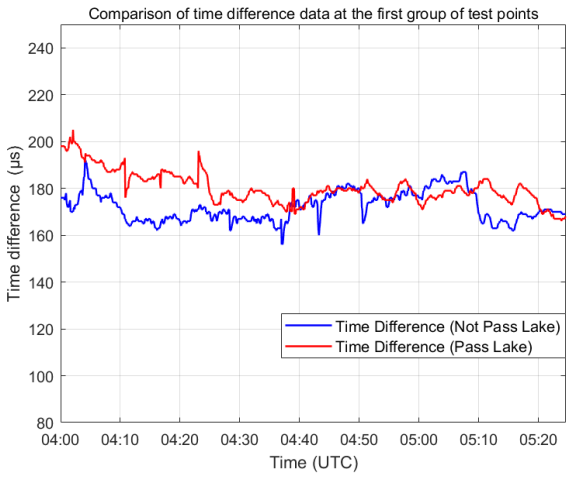

Fig. 8. Comparison chart of the first group of lake water time difference values.

The red curve in the figure represents the field strength results after passing through the lake water, while the blue curve shows the test results without passing through the lake water. The test results for the first group of lake water in the ground wave area are shown in Table 3.

Table 3. Statistics of test data for the lake test within the near-field range (25 km).

Time difference [μs]	Test point 1 Pass lake	Test point 2 Not pass lake
Max value	205.01	191.97
Min value	166.83	155.99
Peak_to_peak	38.18	35.98
Mean value	180.25	172.21
Std	6.86	6.38

As shown in Table 3, the time difference along the lake path is relatively large, being 8.04 μs greater than the average time difference in the direction without passing through the lake path. The detailed test data for the ground wave area are shown in Fig. 8. Both sets of measured data are relatively stable. The differences between the maximum and minimum values are 38.18 μs and 35.98 μs, respectively, and the standard deviations are 6.86 μs and 6.38 μs, respectively. After passing through the lake water, the signal time difference shows a slight fluctuation, and the time difference range also increases accordingly. As this set of test points is relatively close to the broadcasting station, the difference in time difference is not particularly significant.

A time difference comparison test was conducted on the second group, Weishan Lake, and the test results are shown in Fig. 9.

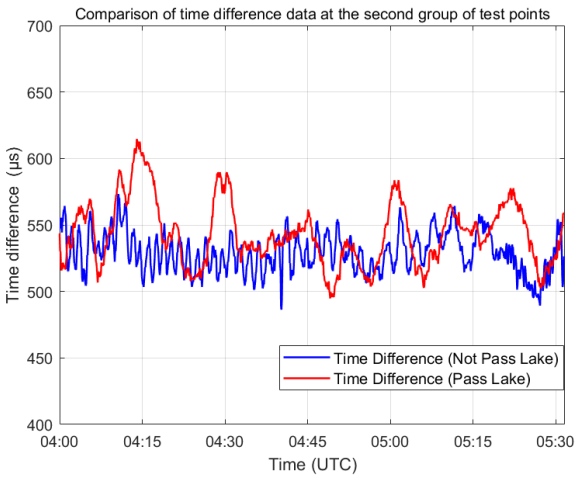

Fig. 9. Comparison chart of lake water time difference values in the second group.

The test results for the second group of lake water in the ground wave area are shown in Table 4.

Table 4. Statistics of test data for the lake test within the ground wave range (138 km).

Time difference [μs]	Test point 1 Pass lake	Test point 2 Not pass lake
Max value	614.69	573.32
Min value	494.51	486.22
Peak_to_peak	120.18	87.10
Mean value	543.17	529.07
Std	24.11	14.97

As shown in Table 4, the time difference along the lake path is relatively large, being 14.1 μs greater than the average time difference in the direction without passing through the lake path. The detailed test data for the ground wave area are shown in Fig. 9. In the figure, the red curve represents the field strength results after passing through the lake water, and the blue curve represents the test results without passing through the lake water. The differences between the maximum and minimum values of the two sets of measured data are 120.18 μs and 87.10 μs, respectively, and the standard deviations are 24.11 μs and 14.97 μs, respectively. This indicates that after passing through the lake, there is a slight fluctuation in the signal time difference, and the range of the time difference also increases.

Signals traversing the lake still exhibit sporadic fluctuations or reflection interference, which may be caused by multipath effects from the lake surface or signal hopping due to water surface fluctuations. This suggests that the lake environment may negatively affect signal stability.

Within the ground wave region, signals maintain stable levels due to the proximity of receiving terminals to broadcasting stations. We conducted experimental studies on signal field strength within the ground wave coverage area at distances ranging from 10 to 300 km from the Shangqiu broadcasting station. By increasing the distance between the timing broadcast station and the receiving location, we analyzed the relationship between distance and field strength to validate the attenuation patterns.

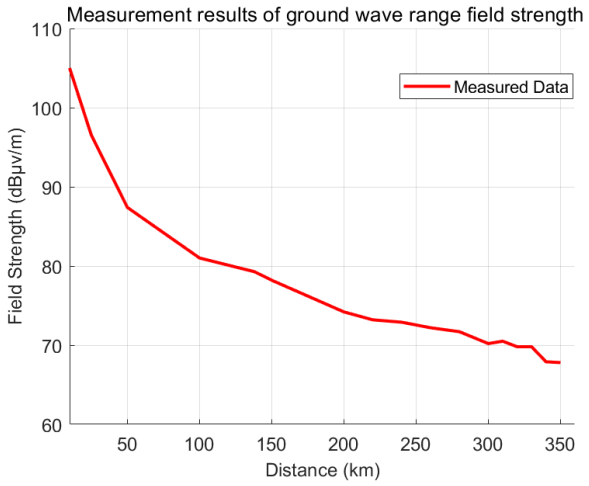

Fig. 10. Variation trend of signal field strength with distance.

As shown in Fig. 10, the field strength at the test point 10 km from the Shangqiu transmitter is 105 dBμV/m, while at 100 km it is 81.01 dBμV/m, indicating rapid attenuation. Between 100 km and 300 km, attenuation becomes nearly linear, decreasing by approximately 0.6 dBμV/m every 20 km. The 300 km to 350 km range falls within the skywave-ground wave interference zone, where the influence of a single skywave hop causes fluctuating attenuation in field strength.

4. Conclusion

This paper presents a lake propagation experiment and test data analysis of BPC timing signals within the ground wave range, yielding the following preliminary results:

1. The study uses the BPC timing signal as an example to examine its transmission and attenuation characteristics in a lake environment and establishes a field strength measurement system based on the principle of field strength measurement for the BPC timing signal. Based on the distance between the transmitting and receiving points in the experimental area, the experiment was conducted in the ground wave area. Two tests with different transmission media and different directions were designed: one with the radio wave signal passing through the lake and the other without passing through the lake. The results of the two groups of experiments show that in the ground wave region, the signal strength attenuation trend is more pronounced when passing through the lake environment than when not passing through the lake, and the attenuation and fluctuation of the field strength value become more significant as the distance between the receiver and the broadcasting station increases. Considering the ground wave range and the relatively short distance between receiving points, it can be assumed that the soil electrical conductivity constants are equal. Therefore, by eliminating the influence of terrain on measurement error, the measurement results are reliable.

2. Lake water is a uniform liquid medium, and the electric field distribution within it is relatively uniform. The conductivity of lake water is much higher than that of soil. Lake water contains large amounts of dissolved salts and other electrolytes, which dissociate into ions in water, allowing it to conduct electricity effectively. Increased moisture enhances the charge conduction capacity of lake water, causing its resistivity to decrease accordingly. In contrast, the conductivity of soil is much lower than that of liquid water, making lake water a much better conductor. At equal distances, the electric field intensity in lake water is usually lower. This is mainly because the high conductivity and uniformity of lake water allow the electric field to be conducted and distributed more easily, while the non-uniformity and complexity of soil can result in higher electric field intensity in certain areas. Highly conductive media are more likely to absorb the energy of electromagnetic waves and convert it into heat, leading to attenuation of the signal field strength.
3. The distribution of electric fields in soil is complex and influenced by factors such as the type, size, shape, and arrangement of soil particles, as well as moisture content and electrolyte concentration in the soil. The porosity and non-uniformity of soil result in an uneven electric field distribution. Differences in conductivity between water and air in the pores also affect the electric field distribution. Increased soil resistivity makes soil a relatively good insulator, causing electric charges to accumulate on and around the soil surface. This charge accumulation alters the electric field distribution of the pure soil medium in the ground wave region, possibly causing the electric field lines to be more concentrated along the soil surface and enhancing local electric field intensity. Soil with high resistivity makes it more difficult for surface charges to diffuse into the atmosphere, leading to greater charge accumulation near the surface and increased electric field strength in that area.
4. In the ground wave region, there is no ionospheric reflection signal. When the propagation distance is fixed, the field strength remains essentially independent of the test time. Research on the loss model of BPC timing signals during lake propagation provides test data to support the future development of underwater timing technology in the PNT timing system of the country. The characteristics and laws of low-frequency deep water and seawater propagation require further study, refinement, and analysis in the next phase.

REFERENCES

[1] Cui, Y. (2013). *Satellite navigation receiver anti-jamming technology research*. Thesis, Tianjin University, Tianjin, China.

[2] Liu, Y. (2023). *Research on the integrity method of GNSS/Loran-C combined timing*. Thesis, Harbin Engineering University, Harbin, China.

[3] Ait-Ighil, M. (2013). *Enhanced physical statistical simulator of the land mobile satellite channel for multipath modelling applied to satellite navigation systems*. Thesis, ISAE-SUPAERO, Toulouse, France.

[4] Wang, Y., Sun, X., Mai, J., Guan, Y., Xu, D. (2022). Review of research on compensation topologies for inductively coupled power transfer systems under variable parameters conditions. In *Zhongguo Dianji Gongcheng Xuebao/Proceedings of the Chinese Society of Electrical Engineering*, 42 (20), 7288-7305.

[5] Liu, X., Zhou, H., Ge, X., Jiao, H. (2024). Development of underwater wireless communication equipment technology. *Strategic Study of CAE*, 26 (2), 38-49. https://www.engineering.org.cn/sscae/EN/10.15302/J-SSCAE-2024.02.006

[6] Zhu, H., Zheng, G., Zhang, H, Zheng, H., Lin, J., Tang, Y. (2017). Study on propagation characteristics of low frequency acoustic signal in shallow water environment. *Journal of Shanghai Jiao Tong University*, 51 (12), 1464-1472. https://doi.org/10.16183/j.cnki.jsjtu.2017.12.009

[7] Yang, S., Liang, J., Ke, X. (2024). Underwater wireless optical communication model and its experimental research progress. *Optical Communication Technology*, 6, 1-5.

[8] Deng, R., Feng, Y., Luo, B. (2016). Underwater optical communication technology difficulty analysis. *Journal of Anhui Technical College of Electronic Information*, 15 (1).

[9] Zhang, H. (2010). *Shallow sea very low frequency sound propagation modeling and research*. Thesis, Harbin Engineering University, Harbin, China.

[10] Teysseyre, P., Briand, C., Marshall, R., Cohen, M. (2025). Effect of ground conductivity on VLF wave propagation. *Radio Science*, 60 (3), e2024RS008150. https://doi.org/10.1029/2024RS008150

[11] Singh, S., Singh, M. (2013). Propagation effects of ground and ionosphere on electromagnetic waves generated by oblique return stroke. *International Journal of Engineering Science Invention*, 2 (4), 43-51.

[12] Korsakov, A. A., Kozlov, V. I., Toropov, A. A. (2020). Seasonal variations of the amplitude of the VLF radio signals and the intensity of the atmospheric electric field in Cryolithozone conditions. *IOP Conference Series: Materials Science and Engineering*, 753, 042093. https://doi.org/10.1088/1757-899X/753/4/042093

[13] Zhao, F., Feng, P., Qi, Z., Cheng, L., Wang, X., Huang, L., Liu, Q., Chen, Y., Ren, X., Hua, Y. (2024). Investigation on the impact of the 2022 Luding M6.8 earthquake on regional low-frequency time code signals in northern China. *Atmosphere*, 15 (12), 1419. https://doi.org/10.3390/atmos15121419

[14] Liu, J. (2002). *The theory and the technique of engineering on low-frequency time-code in time service system*. Thesis, University of Chinese Academy of Sciences, Beijing, China.

[15] Liu, Z. (2007). *The research on applying virtual instrument technology to measure and monitor low-frequency timecodes time service signal*. Thesis, University of Chinese Academy of Sciences, Beijing, China.

[16] Zhao, J. (2007). *Research and design of low-frequency time-code signal field strength measurement method and portable field strength meter*. Thesis, University of Chinese Academy of Sciences, Beijing, China.

[17] Xu, L., Liu, J., Wu, G. (2000). Low frequency code signal when the development of the field intensity meter. *Journal of Shaanxi Astronomical Observatory Station*, 2, 95-101.

[18] Gu, Z. (2012). *Research and design of low-frequency time code receiving system*. Thesis, Nanjing University, Nanjing, China.

[19] Liu, Z., Wu, G. (2010). A New Method for measuring the field strength of low-frequency time-code signals. *Metrology & Testing Technology*, 37 (12), 25-26.

[20] Liu, Z., Wu, G., Feng, P. (2007). Based on virtual instrument of low frequency code transmit signal real-time monitoring system. *Journal of Foreign Electronic Measurement Technology*, 2, 60-62. https://doi.org/10.19652/j.cnki.femt.2007.02.018

Received April 30, 2025
Accepted November 17, 2025